Title:
Measuring Mean Cup Depth in the Optic Nerve Head

Authors:
John K. Johnstone, jkj@uab.edu, Computer and Information Sciences and Ophthalmology, UAB
Lindsay Rhodes, rhodesl@uab.edu, Ophthalmology, UAB
Massimo Fazio, massimof@uab.edu, Ophthalmology, UAB
Brandon Smith, smithbls@uab.edu, Ophthalmology, UAB
Lan Wang, lanwang@uab.edu, Ophthalmology, UAB
J. Crawford Downs, cdowns@uab.edu, Ophthalmology, UAB
Cynthia Owsley, owsley@uab.edu, Ophthalmology, UAB
Christopher A. Girkin, cgirkin@uab.edu, Ophthalmology, UAB

Keywords:
Cup Depth, Modeling of the Internal Limiting Membrane, Bruch Reference Structure, Uniform Sampling

DOI: 10.14733/cadconfP.2015.189-193

Introduction:
Structural changes in the optic nerve head (ONH) have been associated with the development of glaucomatous optic neuropathy, in particular, expansion of the optic cup due to loss of neuroretinal tissues and remodeling of the underlying lamina cribrosa, motivating a quantitative analysis of ONH morphology. Cup depth is a useful measure that reflects the anatomical changes seen in glaucoma [9] and can be calculated based on the shape of the internal limiting membrane (ILM). This paper considers the computation of mean cup depth. Unlike previous studies that have computed cup depth directly from images [10], from few samples [8], or that assess cup depth qualitatively rather than quantitatively [6], we build a full shape model of the ILM from dense point clouds. We also use algorithms from shape modeling to build reference structures and to measure cup depth, as opposed to using manual measurements.

To measure depth, a reference structure is necessary. A reference plane based on Bruch's membrane (BM) has been used in both clinical and histological studies against which to measure depth in the ONH (Fig. 1b,c). The opening of Bruch's membrane (BMO), the inner boundary of Bruch's membrane at the anterior end of the neural canal, is nearly planar and nearly elliptical, making it a good candidate for a reference structure. An alternative reference structure may be defined using the anterior sclera, which might be more stable than the Bruch structure [5]. For simplicity, we use the Bruch reference structure in this extended abstract. *Bruch cup depth* (Fig. 1c) is the signed distance of an ILM point from the best-fitting plane of BMO (called the BMO plane), positive if the ILM point lies on the same side as the lamina cribrosa, which always lies strictly on one side of the BMO plane. Measurement of cup depth should be constrained to the region over the ONH. The BMO again offers a natural mechanism to formalize this constraint: the BMO cylinder is the right elliptical cylinder defined by the best-fitting ellipse of BMO (called the BMO ellipse), and only ILM samples that lie within the BMO cylinder are considered during the computation of cup depth.

The goal of this paper is an algorithm for the computation of mean cup depth, an important and computationally interesting measurement. After describing the structure of an ONH dataset, we discuss mean cup depth and its two major components: computation of the Bruch reference structure that is used to measure depth, and construction of the underlying ILM mesh that is used to sample cup depths. We finish by evaluating the accuracy of our algorithm using synthetic datasets.

Computational aspects:

ONH dataset

The ONH is modeled from an ONH dataset with a unique structure, a collection of several independent point clouds each organized into radial planar sections sharing a rotational axis (Fig. 1a). This is in contrast to the usual structure of point clouds in shape modeling as either unorganized points or point clouds organized into parallel sections (as in CT/MR imaging and topographical maps). A radial slicing is natural for the optic nerve head, since the locus of interest is near the center of the volume, where radial slices concentrate the data. The radial sections are manually segmented from spectral domain optical coherence tomography (SDOCT) images by trained observers (Smith and Wang) [1], yielding separate point clouds for the categories of interest in the ONH: for Bruch cup depth, these are the ILM and BM. The radial sections are oriented consistently by ensuring that the rays from first to last point of consecutive sections differ by less than $\pi/2$. To simplify mesh construction, the oriented sections are split into half-sections at the axis of rotation. The orientation of the second half-section is flipped so that all half-sections end at the axis.

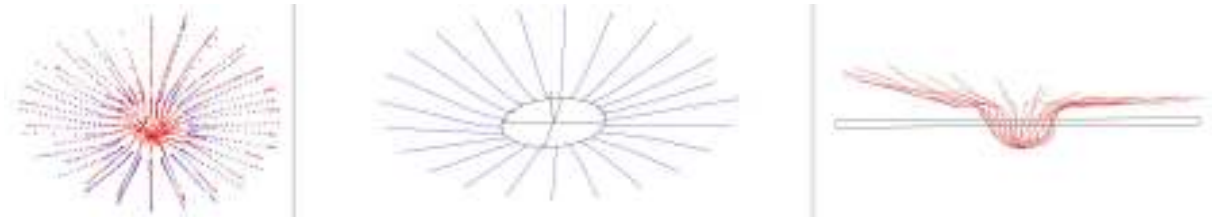

Fig. 1: (a) The internal limiting membrane (red) and Bruch's membrane (blue) point clouds of a typical ONH dataset. Note the radial structure. (b) The Bruch reference structure. The BMO ellipse is shown with the BM (blue). The BMO ellipse lies in the BMO plane. The axis of the BMO cylinder is also shown. (c) Bruch cup depth. The ILM (red) and BMO plane (black): the cup depth of a point of the ILM is its signed distance from the BMO plane.

The radial nature of the ONH dataset leads to some interesting challenges. Care must be taken that sampling is not biased towards the center (if mean statistics are of interest as here), shape degeneracies can exist near the rotational axis, and an ONH dataset does not represent a manifold surface (the sections do not cross the axis at a common point) due to the noise inherent to the segmentation. Fortunately, the topology of the ONH is simple and known, so the challenges are with geometry and not with topology.

Mean cup depth

A robust computation of mean cup depth requires a good sampling of cup depths. An ILM surface (a triangle mesh) is reconstructed from the ILM point cloud and this surface is sampled. Although mean cup depth suggests using a uniform sampling of this ILM surface, a perfectly uniform sampling is impossible (otherwise this sampling would define a regular polyhedron). One idea we tried was to transfer a uniform sampling of parameter space to the mesh using a distortion-minimizing parameterization, as explored in texture mapping [4], but this was challenging and proved inferior to a weighted sampling. We found that an excellent algorithm to compute mean cup depth is to sample at the triangle centroids of the ILM mesh and weight by area:

$$meanCD = \sum_{T} \frac{area(T)}{area(M)} CD(centroid(T)) \tag{2.1}$$

The sum ranges over all triangles T of an ILM mesh M that has been clipped to the BMO cylinder. The construction of the ILM mesh is considered below.

The computation of cup depth is simplified by working in a special coordinate frame. A Bruch frame is a coordinate frame whose origin is the center of the best-fitting ellipse of the BMO, z-axis is normal to the BMO plane, and z>0 half-space is the half-space of the BMO plane that contains the

lamina cribrosa. In a Bruch frame, the cup depth of an ILM point is simply its z-coordinate. Since structural changes in the optic nerve head may be localized, mean cup depth is also measured by quadrant (superior, temporal, inferior, nasal).

Bruch reference structure

The BMO plane and ellipse (Fig. 1b,c) are computed using principal component analysis [2]. Let $B=\{b_1,\ldots,b_n\}$ be the BMO point cloud with mean $\bar{b}$ and covariance matrix $M=\frac{1}{n}\sum_{i=1}^{n}(b_i-\bar{b})(b_i-\bar{b})^t$. The eigenvector of M associated with the smallest eigenvalue defines the normal of the best-fitting plane of B (as the direction of minimal variance of the point cloud) and the best-fitting plane passes through $\bar{b}$. The eigenvector of M associated with the largest (resp., middle) eigenvalue defines the direction of the major (resp., minor) axis of the best-fitting ellipse. Eigenvectors may be computed robustly in C++ using the Eigen numerical library. The BMO ellipse will be fully defined once its axis lengths and center are known. Note that the sample mean is not the center of the BMO ellipse, since the point cloud is not uniformly sampled. Since the BMO point cloud B lies close to its best-fitting ellipse, the axis lengths may be found by projecting B onto each principal axis and using the range of these points to define the semi-axis length. The sample mean $\bar{b}$ is adjusted to the ellipse center by projecting it onto each principal axis, along with the extreme points on that axis, to determine how much $\bar{b}$ must be adjusted to lie midway on each axis.

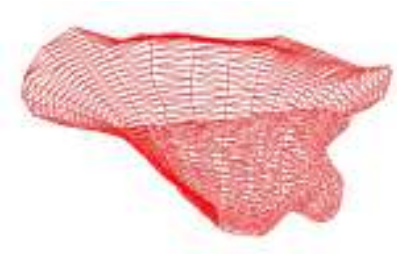

Fig. 2: An ILM mesh, a minimal surface area reconstruction from a resampling of the ILM half-sections.

ILM mesh

A robust ILM mesh (Fig. 2) is required for mean cup depth, and the construction of a robust mesh requires a robust sampling. Sections are oversampled in some areas and undersampled in others, prompting the construction of an interpolating curve before resampling. The oversampling complicates this construction. The solution is to downsample, then interpolate, then upsample. Each ILM section is downsampled, using a variant of Douglas-Peucker decimation: while walking around the section, samples are removed whenever they preserve the invariant that every original sample is within a prescribed distance of the polygon defined by the downsampling. The tolerance is chosen to be .0001 of the radius of the ONH dataset's bounding box. The samples of the downsampled section are reliable for the construction of an interpolating cubic B-spline curve, which is then uniformly sampled for the desired robust sampling. The resampled section is then clipped to the BMO cylinder. A mesh is built from the clipped half-sections using the contour reconstruction algorithm of Fuchs, Kedem and Uselton [3]. This algorithm uses minimal surface area as the constraint, and reduces this optimization to the construction of a shortest path in a toroidal graph built from neighbouring half-sections. Here we see another advantage of using half-sections: they enforce the constraint that points on the axis of rotation must correspond.

Synthetic datasets

An attractive way to evaluate the accuracy of our computation of mean cup depth is by running the algorithm on synthetic datasets for which the correct value can be computed analytically using integration. Various synthetic ILM surfaces were built by sampling mathematical functions that mirror the shape of the ILM: the Gaussian $z = G(x,y,\sigma) = \frac{1}{2\pi\sigma^2} e^{-\frac{x^2+y^2}{2\sigma^2}}$, even Gabor $z = \cos\left(\omega_0\sqrt{x^2+y^2}\right)G(x,y,\sigma)$, odd Gabor $z = \sin\left(\omega_0\sqrt{x^2+y^2}\right)G(x,y,\sigma)$, sinc $z = \frac{\sin\left(\sqrt{x^2+y^2}\right)}{\sqrt{x^2+y^2}}$, and cosine $z = \cos\left(w_0\sqrt{x^2+y^2}\right)$. The BM was built so that the BMO plane and ellipse define a clean domain of integration for the ILM surface. With a small modification to our computation of mean cup depth, replacing the areas in Eqn. (2.1) by the area of their projections onto the BMO plane, our computation reduces to the ratio of a volume to an area: the volume of the ILM under the BMO plane divided by the area of the BMO ellipse. Therefore, this new computation can be compared against a numerical integration using MATLAB, since the ILM is a known mathematical surface. By varying the ILM surface and the size and height of the BMO ellipse, many different synthetic datasets were built and tested.

Tab. 1 compares the result from MATLAB integration with the result computed by our algorithm on a set of synthetic datasets. Along with varying the type of mathematical surface, the parameters of the ILM surface may be adjusted (the standard deviation σ of the underlying Gaussian or the frequency w_0 of the underlying cosine or sine) and the domain of integration may be adjusted (by changing the radius of the BMO cylinder and the height of the BMO plane, parameters r and z in Tab. 1). The percent relative error is also reported: the percent relative error of a computed solution x' from the true solution x is $\frac{100|x'-x|}{|x|}$. All these results are accurate to at least 3 decimal places with very low relative error.

Function	σ	w_0	r	z	MATLAB integration	Our algorithm	% relative error
Gaussian	.7		1	-1	1.2036	1.20359	.00083 %
Gaussian	.5		2	-1	1.0796	1.08042	.076 %
even Gabor	.6	10	2	-.5	.4977	.497726	.0052 %
even Gabor	.8	8	2	-.5	.4979	.498001	.020 %
odd Gabor	.6	10	2	-.5	.4999	.49988	.0040 %
sinc			20	-2	2	2.00303	.15 %
cosine		3	3	-2	2.0444	2.04409	.015 %

Tab. 1: Results on synthetic datasets using integration vs. our algorithm.

Along with this evaluation against synthetic datasets, the components of the C++ code were rigorously tested. An alternative way to build synthetic datasets was also tested, by firing rays at an algebraic surface $f(x,y,z) = 0$.

Conclusions:

Our computation of cup depth has been used to analyze correlations between cup depth, race, and age [7]. This experience with the computation of mean cup depth has revealed the importance of cleaning the data, building a robust surface model for key anatomy, computing a robust reference structure,

and using special reference frames during computation. The centrality of sampling is striking: a robust sampling of the ILM sections leads to a robust ILM mesh, which leads to a robust sampling of cup depths for mean depth.

The potential applications of shape modeling to the morphometry of anatomy are rich. The algorithms for mean cup depth in the optic nerve head developed in this paper are but one case study. In present and future work, we are considering a wider assortment of statistics for ONH morphometry, including volume, thickness, and curvature, and the alignment of a pair of ONH datasets for rigorous quantitative comparison.

Acknowledgements:

Supported by grants from the National Eye Institute (EY018926, EY14267, EY019869), the National Institute on Aging (R01AG04212), the EyeSight Foundation of Alabama, and Research to Prevent Blindness.

References:

[1] Downs, J.C.; Yang, H.; Girkin, C.; Sakata, L.; Bellezza, A.; Thompson, H.; Burgoyne, C.F.: Three-Dimensional Histomorphometry of the Normal and Early Glaucomatous Monkey Optic Nerve Head: Neural Canal and Subarachnoid Space Architecture, Investigative Ophthalmology and Visual Science, 48(7), 2007, 3195-3208. http://dx.doi.org/10.1167/iovs.07-0021

[2] Duda, R.O.; Hart, P.E.; Stork, D.G.: Pattern Classification, Wiley-Interscience, New York, 2001.

[3] Fuchs, H.; Kedem, Z.M.; Uselton, S.P.: Optimal Surface Reconstruction from Planar Contours, Communications of the ACM, 20(10), 1977, 693-702. http://dx.doi.org/10.1145/359842.359846

[4] Hormann, K.; Levy, B.; Sheffer, A.: Mesh Parameterization: Theory and Practice, SIGGRAPH Course Notes, 2007.

[5] Johnstone, J.; Fazio, M.; Rojananuangnit, K.; Smith, B.; Clark, M.; Downs, C.; Owsley, C.; Girard, M.J.A.; Mari, J.M.; Girkin, C.A.: Variation of the Axial Location of Bruch's Membrane Opening with Age, Choroidal Thickness and Race, Investigative Ophthalmology and Visual Science, 55(3), 2014, 2004-2009. http://dx.doi.org/10.1167/iovs.13-12937

[6] Jonas, J.B.; Martus, P.; Budde, W.M.; Hayler, J.: Morphologic Predictive Factors for Development of Optic Disc Hemorrhages in Glaucoma, Investigative Ophthalmology and Visual Science, 43(9), 2002, 2956-2961. PMid:12202515

[7] Rhodes, L.; Huisingh, C.; Johnstone, J.; Fazio, M.;Smith, B.; Clark, M.; Downs, J.C.; Owsley, C.; Girard, M.J.; Mari, J.M.; Girkin, C.A.: Variation of Laminar Depth in Normal Eyes with Age and Race, Investigative Ophthalmology and Visual Science, 2014. http://dx.doi.org/10.1167/iovs.14-15251

[8] Seo, J.H.; Kim, T.-W.; Weinreb, R.N.: Lamina Cribrosa Depth in Healthy Eyes, Investigative Ophthalmology and Visual Science, 55(3), 2014, 1241-1251. http://dx.doi.org/10.1167/iovs.13-12536

[9] Weinreb, R.N.; Khaw, P.T.: Primary open-angle glaucoma, Lancet, 363, 2004, 1711-1720. http://dx.doi.org/10.1016/S0140-6736(04)16257-0

[10] Wells, A.P.; Garway-Heath, D.F.; Pootschi, A.; Wong, T.; Chan, K.C.Y.; Sachdev, N.: Corneal Hysteresis but not Corneal Thickness Correlates with Optic Nerve Surface Compliance in Glaucoma Patients, Investigative Ophthalmology and Visual Science, 49(8), 2008, 3262-3268. http://dx.doi.org/10.1167/iovs.07-1556